Interfacial energy states of moisture-exposed cracks in mica

Kai-Tak Wan,[a] Nicholas Aimard,[b] S. Lathabai,[a] Roger G. Horn, and Brian R. Lawn
Ceramics Division, National Institute of Standards and Technology, Gaithersburg, Maryland 20899

(Received 25 May 1989; accepted 13 September 1989)

Results of crack growth observations on mica in water-containing environments are described. The study focuses on equilibrium crack states for reversed loading cycles, i.e., for initial propagation through virgin solid and subsequent retraction-repropagation through healed or misoriented-healed interfaces. Departures from these equilibrium states are manifest as steady-state forward or backward crack velocities at specific applied loads. The equilibria are thereby interpreted as quiescent, threshold configurations $G = \mathbf{W}_E$, with G the Griffith mechanical-energy-release rate and $\mathbf{W}_E$ the Dupré work of adhesion, on crack velocity (v-G) diagrams. Generally, $\mathbf{W}_E$ is found to decrease with concentration of water, in accordance with a Gibbs formalism. Hysteresis is observed in the forward-backward-forward crack propagation cycle, signifying a reduction in the adhesion energy on exposure of the open interface to environmental species prior to healing. This hysteresis is especially marked for those interfaces that are misoriented before healing, indicating that the structure of the underlying solid substrate as well as of the intervening fluid is an important consideration in the interface energetics. The equilibrium states for different environments can be represented on a simple energy-level diagram, as differences between thermodynamic end-point states: initial, closed-interface states refer to crystallographic bonding configurations ahead of the crack-tip adhesion zone; final, open interface states refer to configurations behind the crack-tip zone. The significance of this diagram in relation to the fundamental atomic structure of interfaces in fracture and other adhesion geometries, including implications concerning kinetics, is discussed.

I. INTRODUCTION

Recent work[1–6] has considered the fundamental interrelationships between "surface" forces and fracture properties of intrinsically brittle solids. It is argued that such forces uniquely determine many critical features, including the role of interactive environmental species, particularly water, in the "laws" of crack growth. For instance, thresholds in crack velocity versus mechanical-energy-release rate (v-G) curves are expressible as "Griffith equilibria",[4,7] formally written as $G = \mathbf{W}$, where $\mathbf{W}$ is the Dupré work of adhesion per unit area of crack interface.[6] The work of adhesion is calculable by integration of the underlying force-separation function for separating planar surfaces with an intervening medium,[4] and may thus be identified explicitly with surface or interface energy terms, 2γ.[4,6,7] In the context of a more general, kinetic description of fracture, "equilibrium" can be interpreted as a quiescent configuration of equal forward and backward fluctuations over discrete (atomic-scale) energy barriers[5,7]; at $G > \mathbf{W}$ and $G < \mathbf{W}$ the crack respectively advances and retracts ("heals") with a rate dependence that defines the crack velocity function.

To some it might seem that this interpretation of the basic conditions for fracture in terms of interplanar forces amounts to little more than an exercise in semantics. After all, the notion of a surface-force function is implicit in the Griffith surface energy formalism. However, it does lead us to a somewhat new physical picture of the way that environmental species enter and interact with the crack interface.[4] In addition, by using an elaborate, "crossed-cylinder" apparatus developed by Israelachvili and co-workers,[8] one can now obtain independent, direct measurements of the force-separation function for two surfaces in an intervening fluid medium. Among the more compelling of the revelations from experiments using this apparatus is that of oscillations in the force-separation function,[9] with periodicity in separation distance close to the diameter of the intervening molecules. Such periodicity is indicative of the existence of metastable equilibrium states associated with a quasi-ordered interfacial fluid structure. The technique has the capacity for determining kinetic states, e.g., by measuring the rate at which the intervening medium is expelled from the mutually approaching surfaces.[10] The opportunity thereby exists for extracting fundamental information on the underlying interactions

[a]Guest scientist on leave from the Department of Materials Science and Engineering, Lehigh University, Bethlehem, Pennsylvania 18015.
[b]Guest scientist on leave from Ecole Superieure de Physique et de Chimie Industrielles de la Ville de Paris, F-75231 Paris.

that predetermine brittle fracture properties; or, conversely, for using fracture as a complementary tool in the study of fundamental surface forces.

Of all the materials that might be adopted as a "model" for investigating the applicability of these surface force concepts to brittle fracture none is better suited than mica which, with care, can be cleaved to atomic-scale smoothness. Because of this smoothness, crack interfaces can be healed over large distances, conveniently allowing examination of crack reversibility. Fracture properties of mica have been documented by groups in the U.S.S.R., U.S.A., and U.K.[11–22] Mica has also been used almost exclusively in the Israelachvili surface force apparatus.[8] Further, it is transparent, so that *in situ* optical observations of the cleavage interface can be made. Finally, its cleavage-plane crystallography is well documented,[23] thus allowing theoretical consideration of the interaction between newly exposed crack surfaces and invasive environmental species.

In this paper we describe the results of crack growth observations on mica crystals in moist (humid air and water) and inert (nitrogen) environments. We confirm that moisture has a deleterious influence on the driving force needed to sustain crack motion at any stage of its loading, as reflected primarily in a reduced value of **W** relative to that for inert conditions. However, our approach differs from that of previous workers in that we determine, where practicable, comprehensive v-G responses, i.e., for reverse crack growth and subsequent repropagation through the healed interface in addition to the initial forward motion through virgin material. The equilibria that determine thresholds are treated as quiescent configurations, where the diffusion rates of intrusion and extrusion of water molecules just balance. These equilibria are shown to be generally metastable, as reflected by hysteresis in the propagation-healing-repropagation cycle. The hysteresis is accentuated for "mismatched" specimens, i.e., specimens in which the cleavage halves are healed back after full separation and rotation about a common surface normal. The attendant interface adhesion energies are most conveniently represented as differences between well-defined thermodynamic end-point states on an energy-level diagram: initial, "closed-interface" states relate to quasi-crystallographic bonding configurations ahead of the nominal crack tip; final, "open-interface" states relate to free surface configurations behind the crack tip. The former are, in principle, determinable from solid-state bonding and defect chemistry, the latter from surface chemistry and physics. Implications of these results in terms of the surface force models alluded to above are considered, particularly in relation to molecular size effects at constrained interfaces.

II. EXPERIMENTAL

Fracture experiments were conducted on Muscovite mica specimens using a double-cantilever beam geometry[3] (Fig. 1). The specimens were prepared by first cleaving $\approx$100 μm thick lamellae from the as-supplied material (Spruce Pine Mica Co., Spruce Pine, North Carolina). These lamellae were diamond-sawn with a fine (25 μm thick) blade into rectangular sheets 25 mm $\times$ 10 mm, after clamping between protective glass blocks to minimize cutting damage at the edges. A fine needle was then used to start a cleavage fissure close to the center plane of each specimen. A polished straight-edged steel strip $2h$ = 50 μm thick (measured to within $\pm$0.5 μm using a precision laser ruler) and width slightly larger than that of the specimen was subsequently inserted to wedge open a crack. Examination of the resulting crack interfaces by optical microscopy served to screen out potentially "unsatisfactory" specimens, viz., those with prominent cleavage steps, scratch marks from the wedge, or edge fissures, where crack "hang-up" (as indicated by irregularities at the front) can occur. More precise measurements of the thicknesses d_1 and d_2 of the two cleavage arms were made (again within $\pm$0.5 μm by laser ruler) at the conclusion of each experiment, i.e., after complete separation of the fracture specimen.

The specimen-wedge system was clamped into a fixture for observing the subsequent crack motion. The fixture was enclosed in a stainless steel environmental chamber, which in turn was mounted onto the stage of an inverted microscope. This arrangement allowed the crack to be observed at all stages of the experiment, either directly through the microscope eyepiece or "post mortem" by video recorder.

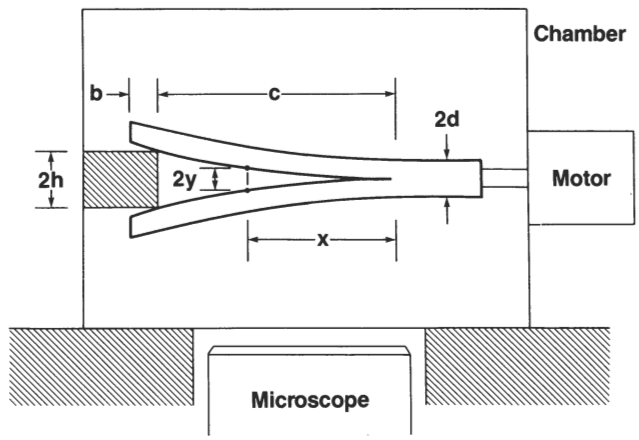

FIG. 1. Schematic of cleavage arrangement. Assembly is enclosed in environmental chamber and seated on microscope stage. Crack motion is effected by translating the specimen relative to the clamped wedge, via the stepper motor. Crack interface is monitored through microscope eyepiece, with facility to record image on VCR.

The atomically smooth cleavage surfaces of mica provide ideal conditions for observing the crack interface. A two-beam Fizeau fringe system is generated at the inner crack walls. By regarding the arms of the cantilevers as thin linear elastic beams,[3,7] it can be shown that the crack profile $y(x)$ in the fringe region may be described by the (inverted) parabolic relation

$$2y = 3hx^2/c^2 \quad (1)$$

with c the crack length and h the wedge thickness. Fizeau interference fringes are seen at separations $2y = m\lambda/2$, where m is the fringe order for constructive interference and λ is the light wavelength (green light in our experiments). With our setup the crack front could be located by extrapolating the data for fringe position to $m = 0$ (typically, for a crack of length $c \approx 1$ mm in laboratory air, to within ± 10 μm).

Crack motion was effected by translating the specimen via a stepper motor drive, with the wedge clamped. The stepper motor could be driven either forward or backward at controlled velocities between 1 and 1000 $\mu m \cdot s^{-1}$. By driving the specimen, the wedge remains stationary in the field of view of the microscope, making measurement of c relatively straightforward. In general, the crack moves at an absolute velocity

$$v = d(b + c)/dt = v_b + v_c \quad (2)$$

with b the wedge penetration (Fig. 1), v_b the corresponding velocity of the stepper motor, and v_c the "apparent" crack velocity in our moving-specimen reference frame. In practice, velocities were most conveniently evaluated from frame-to-frame measurements of the crack-front position on the video tape recordings.

As stated in Sec. I, the primary aim was to evaluate equilibrium crack states in prescribed moisture-containing environments. Such equilibrium states are properly identified in our experiments as zero velocity configurations on v-G curves, i.e., threshold states $G = \mathbf{W}$, where G is the mechanical-energy-release rate. G is evaluated from the well-documented thin-beam cantilever formula[7]

$$G = 3Eh^2\bar{d}^3/4c^4 \quad (3)$$

with E Young's modulus and $\bar{d}$ the suitably "averaged" beam half-thickness: $2/\bar{d}^3 = 1/d_1^3 + 1/d_2^3$ for asymmetrical beams. The sensitivity of G to h, $\bar{d}$, and c demands attention to accuracy in measurements; with the precision levels quoted above, G could be determined to an accuracy of better than 10%.

Tests with this arrangement were run at room temperature (25 °C) in the following environments: dry nitrogen gas (maintained by streaming through chamber inlet); controlled laboratory air, with most tests at relative humidity 60% but others over the range 3 to 90%; distilled water (by immersing the entire specimen). Each new test environment was admitted to the chamber at least 15 min before actual specimen loading. Two basic loading modes were adopted:

Mode (i). The stepper motor drive was activated at maximum speed for a prescribed interval, thereby advancing the crack abruptly into the specimen. The subsequent decaying crack growth at b = const. was then followed simply by monitoring c ($v_b = 0$, $v = v_c > 0$), thus allowing the v-G curve to be determined under conditions of monotonically decreasing G [Eq. (3)]. By reversing the motor drive the crack could be unloaded ($v_c < 0$) and reloaded at will, thus enabling analogous healing and repropagation v-G curves to be determined.[3] Most of the data were collected using this drive mode.

Mode (ii). The motor drive was maintained at constant speed at each velocity measurement. The practice of moving the specimen rather than the wedge was particularly advantageous in this mode; a stationary crack front in the field of view of the microscope ($v_c = 0$, $v = v_b$ = const.) then ensures that a steady-state value of G has been attained. This drive mode was useful for exploring potential artifacts in the data from transient states.

Some comparative tests were conducted on specimen halves that had been cleaved to completion, separated, mutually rotated about a common surface normal, and brought back into a mismatched adhesion state.[17]

III. RESULTS

Results of our observations are presented on v-G diagrams in Figs. 2–4. Logarithmic velocity coordinates in these diagrams are used in order to accommodate the data range. Separation of Fig. 3 into upper and lower halves is to distinguish between forward and backward crack velocities. Symbols in this same figure indicate various branches of the loading cycle: O+, initial loading, forward crack motion into virgin material; H−,

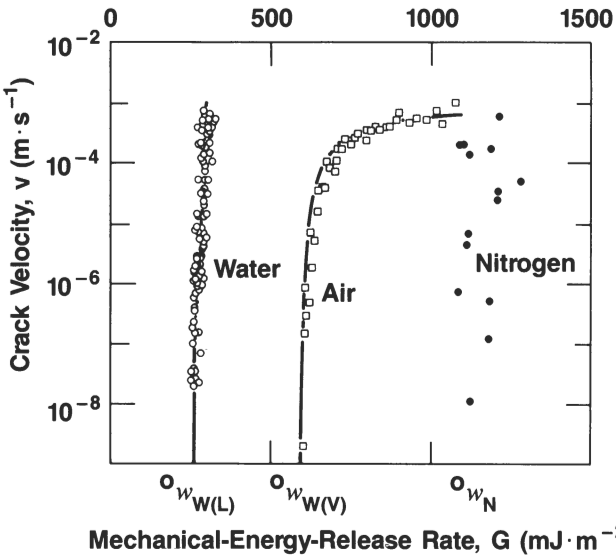

FIG. 2. Crack velocity versus mechanical-energy-release rate for cracks propagating into virgin mica (O+ curves) in nitrogen gas, air (50–60% relative humidity), and water.

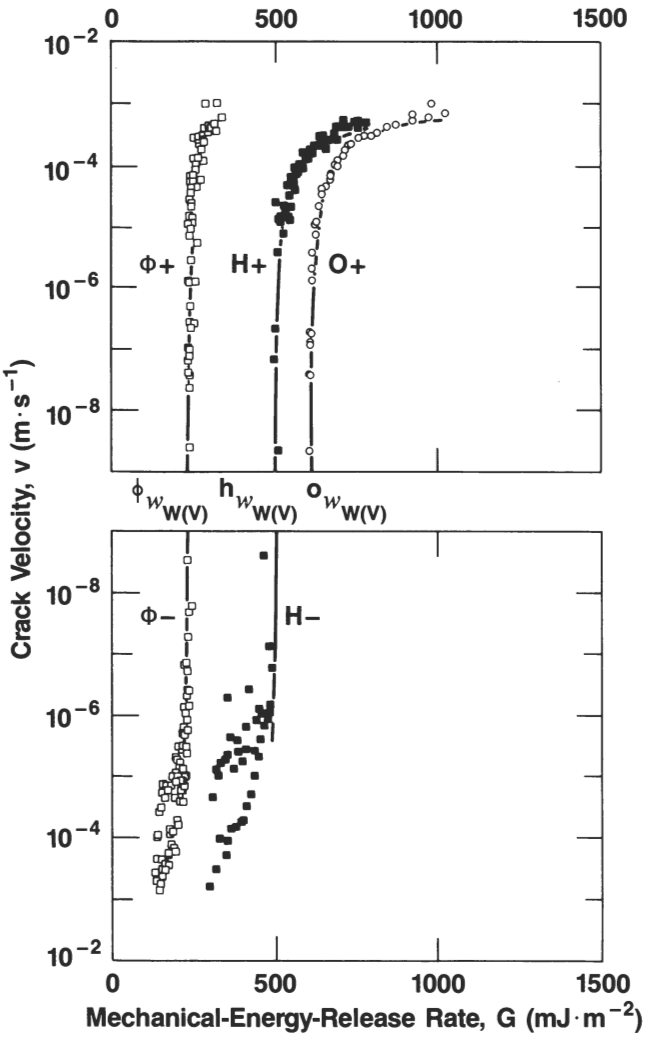

FIG. 3. Crack velocity versus mechanical-energy-release rate for cracks propagating in mica in air (50–60% relative humidity). Upper segment, forward velocities; lower segment, negative velocities. Loading into virgin material (O+); unloading-reloading along healed interface (H−/H+); same but after separating cleavage halves and misorienting about common surface normal (Φ−/Φ+).

unloading, reverse crack motion with healing; H+, subsequent forward reloading through healed region; Φ−, unloading but after misorienting mica sheets; Φ+, reloading after misorientation. (In the H+ tests care has to be taken to ensure that the crack does not extend beyond the position of the original front achieved in the initial loading phase, i.e., into virgin material.) The curves through the data in Figs. 2–4 are theoretical data fits based on a detailed analysis of the fracture kinetics, to be described elsewhere[24] (see also Sec. IV.C). We include these fitted curves here solely to emphasize the distinctive approach of the *v-G* data to threshold.

Three basic sets of experiments were carried out:

(i) In the first set, comparative initial forward loading (O+) tests were conducted in nitrogen gas, laboratory air (50–60% relative humidity), and water, to investi-

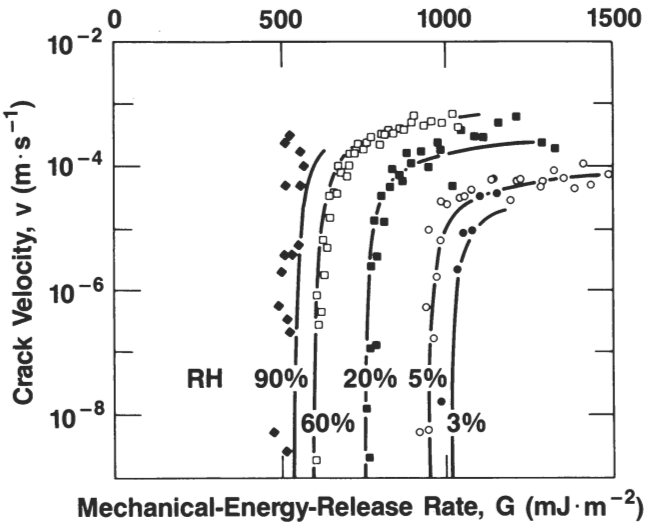

FIG. 4. Crack velocity versus mechanical-energy-release rate for cracks propagating into virgin mica in moist air (O+), at different relative humidity (RH).

gate the general influence of environmental species. To avoid potential uncertainties from systematic specimen-to-specimen error (see below), we include in Fig. 2 results from several sequential runs on just one sheet of mica. Care was taken to flush the chamber thoroughly with each new environmental species between runs to avoid transient effects associated with residual trapped species at the crack interface. This was most conveniently done by starting each run in mode (ii) motor drive at low velocity (usually <20 μm · s^{-1}) until a steady-state configuration was achieved, at which point the system was switched to mode (i) drive and data collection started. In nitrogen the crack growth was highly erratic, as manifested by unstable jumps in growth and ever-changing undulations along the front, typically on a scale of 100 μm or so over a crack length $\approx$1 mm. Such erratic behavior has been previously attributed to surface-charge domain effects.[12,13,15,16,20] Attempts were made to restrict crack length measurements to lower energy configurations where the magnitude of such jumps was minimal, and even then the results were highly irreproducible. Growth in moist air and water, by contrast, was relatively smooth. Nevertheless, with water care was taken not to leave the system standing for excessive intervals before starting the crack, in case of buildup of interlayer corrosion products.[25]

The deleterious effect of water species is clearly manifest in Fig. 2 as a systematic shift in the data to lower threshold *G* values.

(ii) The second set of experiments was aimed at investigating potential changes in the energy states at the healed mica-environment-mica interface relative to the virgin mica-mica interface. Accordingly, data are shown in Fig. 3 for O+, H−, H+, Φ−, and Φ+ loading

runs in laboratory air, on a different specimen to that used in Fig. 2. Air was the most favorable environment for these tests; healing was almost always guaranteed, and reproducible, in this environment. In nitrogen and water, healing occurred on only exceptional occasions: in nitrogen, success appeared to be fortuitous, apparently depending on the degree of surface charging; in water, healing in both matched and mismatched specimens seemed to be hindered by the most minor of interfacial obstructions, especially edge roughness, suggesting a low residual adhesion (although a higher incidence *could* be induced by running the crack at high forward and reverse wedge speeds, e.g., 1000 $\mu m \cdot s^{-1}$, and small intervals, typically <10 s, between half-cycles). Generally in these last two environments the Fizeau fringe pattern at the unloading interface tended simply to expand [$c + b = \text{const.}, v_b < 0, v_c > 0$; i.e., c increasing in Eq. (1)] rather than translate rigidly backward ($c = \text{const.}$), indicating mere crack closure rather than healing. The data in Fig. 3 were again taken on a single specimen, but in this case an unlimited number of H−/H+ and Φ−/Φ+ cyclic runs could be made.

It would appear from the results in Fig. 3 that there exists a common threshold for the H− and H+ half-cycles, and similarly for the Φ− and Φ+ half-cycles. We note an apparent, small hysteresis between the O+ and H curves. The hysteresis between the O+ and Φ curves is substantially larger. Exposure of the surfaces to water vapor before healing thus lowers the threshold G level, but not as much as does misorientation of the cleavage halves.

(iii) The third set of experiments was carried out to confirm the influence of moisture content. Figure 4 shows data for moist air at selected relative humidities, from two further specimens, for forward loading (O+) tests. The shift to lower thresholds with increasing partial pressure of water vapor is again evident.

Since the primary concern in the present paper is with equilibrium interfacial energy states, we focus our attention on the steep portions of the v-G curves in the threshold region. The threshold ($G = \mathbf{W}$) states in Figs. 2–4 are determined as intersection points at $v = 0$. We distinguish between adhesion energies for various interfacial configurations by means of an appropriate superscript-subscript notation, e.g., $^{\circ}\mathbf{W}_{BEB}$, abbreviated here to $^{\circ}\mathbf{W}_{E}$. Superscripts on the left denote the state of the closed crack interface: ∘ virgin, h healed, ϕ rotated prior to healing. Subscripts on the right denote the material-environment system: E environment at the open crack interface—specifically, N nitrogen and W water in liquid (L) or vapor (V) form; B solid body, henceforth omitted on the strict understanding that we are always dealing with the same solid (mica) on either side of the interface. Because of the hysteresis, there is an element of subjectivity associated with determination of the respective adhesion terms from Figs. 2–4. $^{\circ}\mathbf{W}_{N}$ and $^{\circ}\mathbf{W}_{W}$ must be determined from the O+ curves in the v-G plots by data extrapolation; the corresponding terms for $^{h}\mathbf{W}_{W}$ and $^{\phi}\mathbf{W}_{W}$ can be evaluated from the H and Φ curves more accurately by interpolation. Again, more detailed analysis of the theoretical basis of these determinations will be given elsewhere.[24]

We alluded above to specimen-to-specimen scatter. Means and standard deviations were determined for the adhesion energy evaluations in air (50–60% relative humidity) and water environments. The relatively erratic behavior in nitrogen made a similar averaging approach impracticable; instead, we simply quote here the lower range of values encountered, as indicated above. For the air data, the scatter is such that the energy error limits for the O and H data practically overlap, reinforcing our earlier conclusion from Fig. 3; i.e., that the reduction of interfacial adhesion energy due to exposure of water vapor during crack advance and retraction is, if significant, indeed small. Lastly, for Φ interfaces in water we assume a zero value for the energy, as an indicator of an immeasurably low adhesion in our experiments.

Table I shows the adhesion energy terms thus obtained, along with comparative values from studies by other groups. There is a clear laboratory-to-laboratory spread. Part of this spread may be attributable to differences in materials, part to variants in experimental methodology. Moreover, it is not always certain that proper efforts have been made to ensure a true state of equilibrium. It is interesting to note that concerted efforts have been made by one source[20] to achieve a near-equilibrium state for nitrogen environments, by using de-ionization sources in the experimental chamber, whence values at the low end of the quoted range in Table I are obtained.

IV. DISCUSSION

Our work is consistent with the notion that thresholds on v-G diagrams are "equilibrium" points ($G = \mathbf{W}$, Table I). It is immediately evident from Fig. 2 that water is deleterious to the adhesion energy, i.e., $^{\circ}\mathbf{W}_{N} > {}^{\circ}\mathbf{W}_{W(V)} > {}^{\circ}\mathbf{W}_{W(L)}$. However, we see from Fig. 3 that the equilibrium depends on the history of the interface as well, $^{\circ}\mathbf{W}_{W(V)} > {}^{h}\mathbf{W}_{W(V)} > {}^{\phi}\mathbf{W}_{W(V)}$, implying that some of the equilibria are metastable. Some interesting questions follow. Mica is generally regarded as inert to chemical attack in aqueous solution, so how is it that water molecules influence the growth in virgin material so strongly?; i.e., why is $^{\circ}\mathbf{W}_{W}$ substantially smaller than $^{\circ}\mathbf{W}_{N}$? Then, why is the propagation-repropagation hysteresis so sensitive to the history of the interface?; i.e., why is $^{h}\mathbf{W}_{W(V)}$ only marginally less than $^{\circ}\mathbf{W}_{W(V)}$, yet $^{\phi}\mathbf{W}_{W(V)}$ much less than $^{\circ}\mathbf{W}_{W(V)}$? It is the nature of these fracture equilibrium states, and their relation to surface forces, that provides our focus for discussion.

TABLE I. Threshold surface work terms $\mathbf{W}_E$ from present experiments (bold type: means and standard deviations). Values from other sources included for comparison (ordinary type). Superscripts denote closed interface state: ∘ virgin, h healed, and ϕ rotated prior to healing. Subscript E denotes environmental species, N nitrogen and W water (vapor V, liquid L).

	${}^{\circ}\mathbf{W}_E$ (mJ · m^{-2})	${}^{h}\mathbf{W}_E$ (mJ · m^{-2})	${}^{\phi}\mathbf{W}_E$ (mJ · m^{-2})	Ref.
$N(V)$ (Or vacuum)	**1000–2000**			
	10 000			15
	960–16 000			20
$W(V)$ (Air) RH = 55%	**608 ± 56**	**500 ± 42**	**235 ± 30**	
	550			13
	580			16
	440		240	17
	760			20
$W(V)$				
(Air) RH = 90–95%	**470 ± 42**			
75–85%	**582 ± 23**			
65–72%	**615 ± 61**			
50–60%	**633 ± 56**			
31–38%	**643 ± 44**			
15–22%	**781 ± 39**			
10–15%	**745 ± 45**			
3– 5%	**950 ± 34**			
$W(L)$ (Distilled water)	**276 ± 55**	**220 ± 40**	≈0	
	250			13
	214			17

A. Fracture thresholds and equilibrium interfacial states

Let us first construct a formal, if qualitative, potential- and force-separation diagram for a solid/fluid interface in the traditional continuum description of matter.[5] We assume that the fluid is noncondensable; no capillary is formed at the crack tip. Figure 5 plots $U(y)$, the free energy per unit area, and $p(y) = +dU(y)/d(2y)$, the corresponding wall-wall force. (Following fracture mechanics convention, we use the positive sign to designate an attractive cohesive force.) The solid curves represent separation in an interactive environmental medium, the dashed curves in vacuum. From the standpoint of defining surface and interface energies (γ terms), it is convenient to designate the primary bonding state in the virgin solid as "ground state" 0, equivalent to setting zero energy level at the minimum in the potential function. The work of adhesion ${}^{\circ}\mathbf{W}_E$ is defined as the work to translate the system along the solid curve from initial (virginal closed) state at $2y = b_0$ to final (adsorbed open) state at $2y = \infty$. Since such an operation essentially creates two new solid-environment (B-E) interfaces from the original virgin solid, this work is identifiable with the corresponding interfacial energy (${}^{\circ}\mathbf{W}_E = 2\gamma_{BE}$).

Now we may arrive at the same final state by considering the following alternative path: (i) Begin with virgin solid (initial ground state, ${}^{\circ}U_i = 0$); (ii) Separate body (B-B) halves from $2y = b_0$ along dashed curve to $2y = \infty$, in vacuum (or, more strictly, in equilibrium with its own vapor), at cost of intrinsic surface energy of solid (intermediate state, $U = 2\gamma_B$); (iii) Allow environmental medium to enter the system and adsorb onto free surfaces, corresponding to transition from dashed to full curve, with gain in adsorption energy (final, two-surface state, $U_f = 2\gamma_B - 2\Delta U_{Ad}$).[26] Since the two paths have the same end points, we may write

$$
\begin{aligned}
{}^{\circ}\mathbf{W}_E &= U_f - {}^{\circ}U_i = U_f = 2\gamma_{BE} \\
&= 2\gamma_B - 2\Delta U_{Ad} = {}^{\circ}\mathbf{W}_0 - 2\Delta U_{Ad}
\end{aligned}
\tag{4}
$$

where ${}^{\circ}\mathbf{W}_0$ is the work of adhesion in vacuum. Equation (4) is a form of the Dupré equation.[26] It is a statement of the fact that, in a reversible process, the cohesion of a solid will generally be lowered by the environmental interaction. This concept of a reduced resistance to surface formation was first invoked in the context of brittle fracture by Orowan.[27] In terms of the correspondingly diminished force function $p(y)$ in Fig. 3, the effect may be likened to a "screening" of the primary surface interactions by the intervening medium.

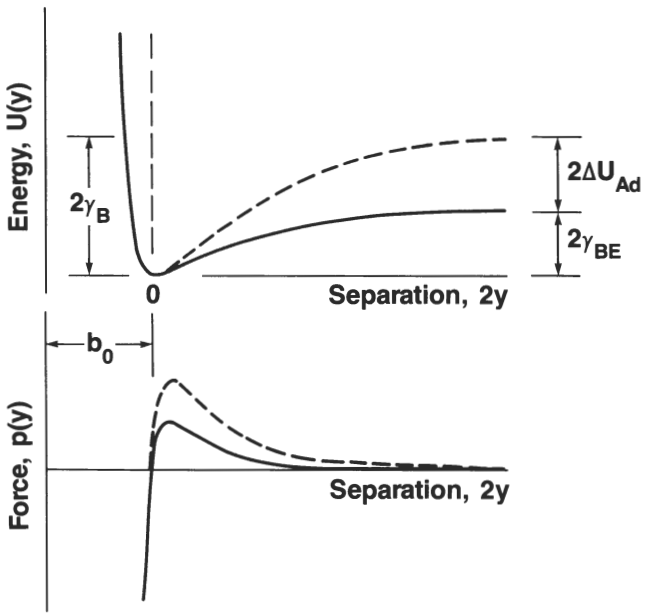

FIG. 5. Potential energy and corresponding surface force function for (unit area) continuum crack system. Solid curves pertain to crack propagation in fluid medium. Dashed curves correspondingly pertain to crack propagation in vacuum. Potential minimum (zero force) taken as "ground state" 0. Note all surface and interface energy (γ) terms are defined relative to this ground state. Effect of environment is to lower effective surface energy and thus to "screen" wall-wall attractions.

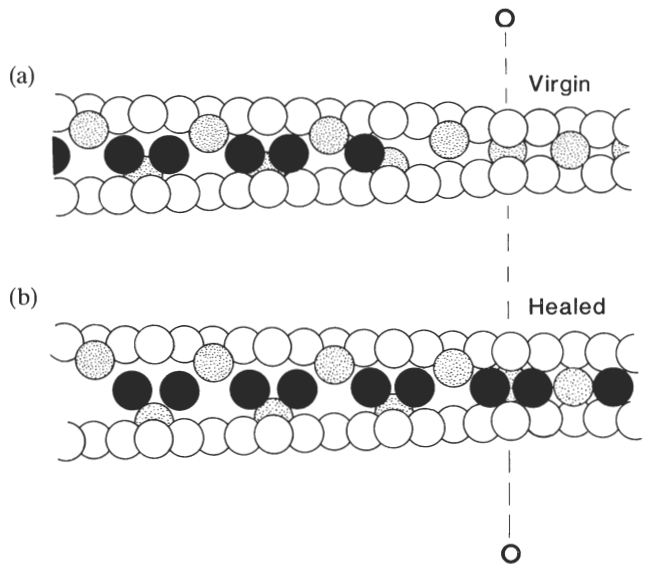

FIG. 6. Crack profiles in mica, computed from "Irwin" elastic displacement field with origin (crack tip) at O-O. Cleavage occurs between oxygen layers (open circles), linked by potassium ions (shaded circles). Water molecules (dark circles) are allowed to penetrate interface to point of equilibrium accommodation. (a) Loading at $G = 200\ \text{mJ} \cdot \text{m}^{-2}$, showing restricted penetration of water molecules along virgin interface; (b) unloading at $G = 100\ \text{mJ} \cdot \text{m}^{-2}$, showing entrapment of water molecules at healed interface. After Ref. 4.

However, the construction in Fig. 5 is necessarily oversimplistic. It presumes complete reversibility in the intrusion and extrusion of fluid at the opening and closing interfaces. As such, the description contains no provision for metastable states. Thus it cannot account for the O/H and O/Φ hysteresis in Fig. 3. Essential elements of discreteness in the crack-interface structure have been excluded from the description.

At this point it is appropriate to refer to theoretical considerations of the crack interfacial structure in mica (and other brittle solids) presented in an earlier study.[4] Figure 6(a) shows a virgin near-threshold interface with intrusive water molecules. The wall separation remains small over a considerable "adhesion zone length" behind the nominal crack tip, well within the range of surface forces measured in the Israelachvili apparatus for aqueous solutions. It is apparent that, contrary to expectation from the continuum descriptions, the intruding molecules cannot diffuse along the interface without significant impedance. Thus on closure these molecules may become entrapped, as shown for the healed interface in Fig. 6(b). The discreteness of the structure in this narrow interfacial configuration then dictates an ordered "occlusion" configuration for the water molecules, i.e., a preferred accommodation of one or more layers at the closed interface, as implied by the oscillatory features in the surface-force function measured in the crossed-cylinder apparatus.[9,28]

Accordingly, consider the modified, "quasi-discrete" energy functions in Fig. 7.[4,5] The dashed curve with primary minimum at 0 again represents the intrinsic cohesion (no environmental interaction); the solid curve with subsidiary minima 1, 2, ... represents the environmentally modified adhesion with integral numbers of intrusive molecular layers between the walls, the broken curve likewise for misoriented walls. Suppose we first retrace the path described earlier in relation to Fig. 5: begin with virgin solid at ground state 0, separate halves to infinity in vacuum, and adsorb onto the walls ($U_f = 2\gamma_B - 2\Delta U_{Ad}$). We note that misorienting the surfaces through ϕ at infinite separation costs no extra energy. Now consider what happens as we close the surfaces, along either the lower solid curve or the upper (misoriented) broken curve. The system has to overcome energy barriers, and, unless infinite time is allowed for thermal fluctuations to restore the intrinsic state at 0, will become trapped in one or another of the subsidiary minima, $U(b_1)$ say, ($b_1 > b_0$). Hence the initial energy state for reopening the surfaces is higher than the ground state by an amount equal to the work of formation of the interface with occluded species E ($^hU_i = \gamma_{hE}$, healed interface; or $^\phi U_i = \gamma_{\phi E}$, misoriented-healed interface). Defining the energy of adhesion in the usual way as the work to translate the system along the appropriate oscillating curve in Fig. 7, we obtain

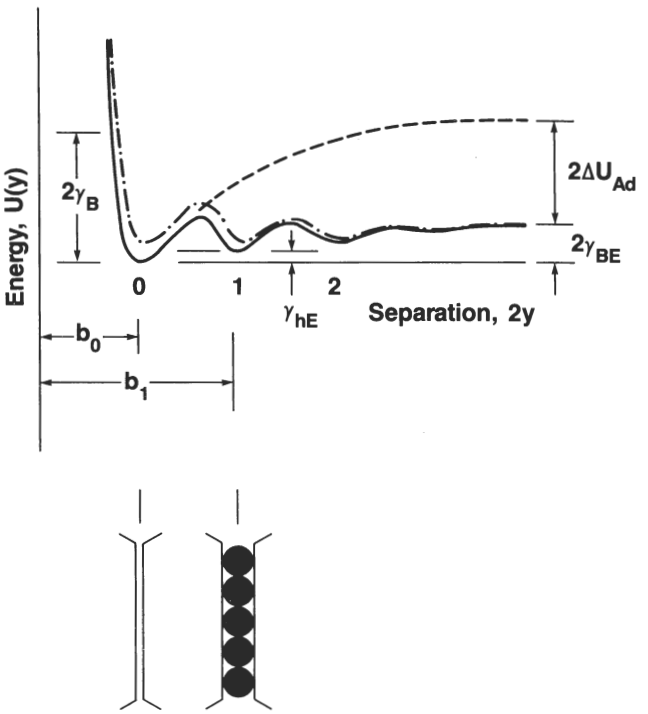

FIG. 7. Potential energy function for (unit area) quasi-discrete crack system in fluid medium. Solid and broken curves represent interfaces in presence of environment, for matched and mismatched surfaces, respectively; dashed curve is for matched interfaces in absence of environment (from Fig. 5). Subsidiary minima 1, 2, etc. in $U(y)$, corresponding to integral numbers of molecule layers, allow for possibility of metastable equilibrium states.

$$ {}^{h}\mathbf{W}_E = U_f - {}^{h}U_i = 2\gamma_B - 2\Delta U_{Ad} - \gamma_{hE} $$
$$ = 2\gamma_{BE} - \gamma_{hE} \quad (5a) $$
$$ {}^{\phi}\mathbf{W}_E = U_f - {}^{\phi}U_i = 2\gamma_B - 2\Delta U_{Ad} - \gamma_{\phi E} $$
$$ = 2\gamma_{BE} - \gamma_{\phi E} \quad (5b) $$

in analogy to Eq. (4).

B. Energy-level diagram

The implication from the hypothetical cycles in Figs. 5 and 7 that the work of adhesion measured in fracture experiments may be expressed simply as a difference between "end-point" equilibrium (or quasi-equilibrium) states lends itself to a conceptually simple energy-level diagram. Such a diagram is constructed for mica in Fig. 8, using values of $\mathbf{W}_E$ from Table I. Energy levels are marked on the vertical axis. Ground state 0 refers, as above, to the relatively well-defined primary bonding configuration of the virgin mica cleavage plane, ${}^{\circ}U_i = 0$. Final states, evaluated from $U_f = {}^{\circ}\mathbf{W}_E$ [Eq. (4)], are plotted on the left: these define the open-surface (implicitly stable) configurations behind the crack-tip adhesion zone. Initial states, evaluated from ${}^{h}U_i = {}^{\circ}\mathbf{W}_E - {}^{h}\mathbf{W}_E$ [Eqs. (4) and (5a)] or ${}^{\phi}U_i = {}^{\circ}\mathbf{W}_E - {}^{\phi}\mathbf{W}_E$ [Eqs. (4) and (5b)], are plotted on the right: these define the closed-

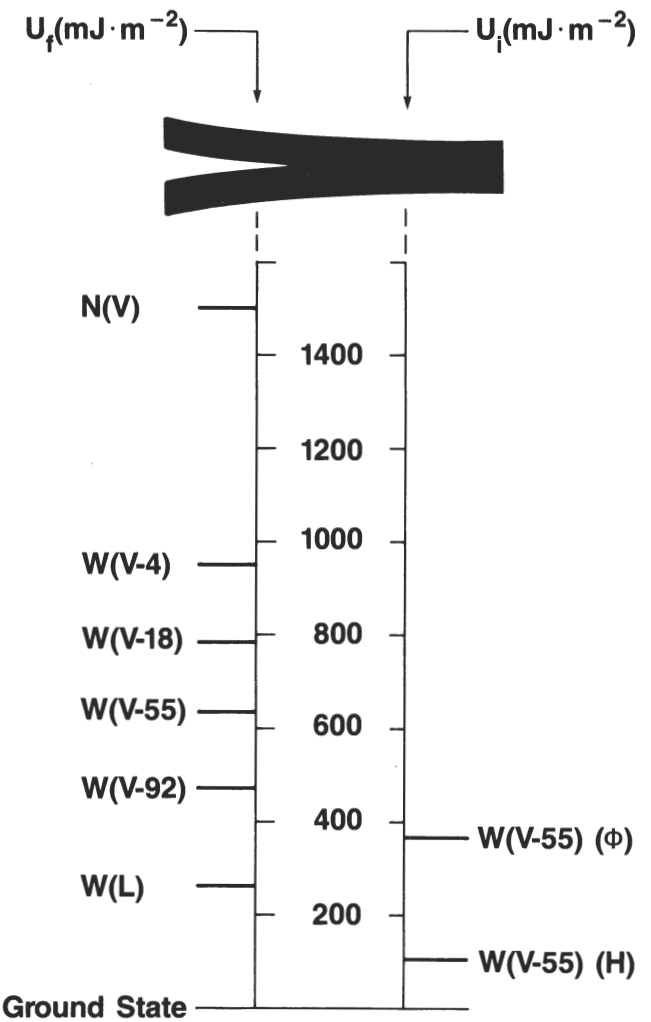

FIG. 8. Energy-level diagram for fracture of mica in moist environments: nitrogen, N; water vapor in air, $W(V)$, at designated relative humidities; water, $W(L)$. Energies correspond to unit area of interface, relative to virgin primary bonding (ground) state. Left side represents final, open-interface states; right side represents initial, closed-interface states. Adhesion energies for virgin interface may be determined directly from left-hand axis, ${}^{0}\mathbf{W}_E = U_f$; for healed (h) interface from the difference in energy levels, ${}^{h}\mathbf{W}_E = U_f - {}^{h}U_i$; similarly, for misoriented-healed (Φ) interface from ${}^{\Phi}\mathbf{W}_E = U_f - {}^{\Phi}U_i$.

interface (stable or metastable) "faulting" configurations ahead of the crack-tip adhesion zone. The work of adhesion for any given environment can now be read off directly as the difference between energy levels on opposite sides of the diagram.

Let us examine the physical nature of these end-point energy states more closely:

(i) Closed, faulted-interface states. The occluded crack interfaces are metastable planar "lattice defects" and, as such, fall within the realm of solid-state defect chemistry. Insertion of an ordered layer of foreign atoms or molecules into a periodic structure leads to a quasi-crystallographic configuration somewhat akin to an extrinsic stacking fault, energy ${}^{h}U_i = \gamma_{hE}$ [cf. Eqs. (4) and

(5a)]. With additional mutual rotation of the upper and lower crystal halves this configuration assumes some of the character of a twist grain boundary, energy ${}^{\phi}U_i = \gamma_{\phi E}$ [cf. Eqs. (4) and (5b)]. Such defect structures at healed crack interfaces in other brittle materials, notably sapphire, have been strikingly imaged by fault diffraction contrast in the transmission electron microscope by Hockey.[29] Evaluations of the fault energies could, in principle, be determined theoretically by summation over pairwise interatomic forces at the interface, but this would require extreme care in assigning sites to the water molecules in relation to the potassium ions,[4] as well as a certain ingenuity in establishing suitable potential functions for the complex electrostatic interactions between these molecules and the mica constituents. An early precedent for such computations was set by Gaines and Tabor,[30] who simplistically treated the water species as dielectric layers between mica slabs with discrete ionic charges. A recent calculation[31] of grain boundary energies for crystal halves with thin ($\approx$1 nm) intervening amorphous phases, using continuum representations of ordered intersurface interactions, is an elaboration of this kind of quasi-discrete approach. Now, first attempts are being made at full-scale molecular statics analyses of hydrolyzed crack interfaces on computers.[32] It is interesting to note that more rigorous molecular statics computations for "simple" twist boundaries (i.e., without intervening water) in ionic solids like MgO suggest that misorientation of a few degrees is sufficient to negate most of the intrinsic Coulombic binding[33]—the bulk of the adhesion in such cases must come from secondary, dipolar interactions. This last suggestion is consistent with the proposition that, whereas inclusion of one or two layers of water molecules in itself may not be sufficient to screen out the Coulombic interactions in mica, an added misorientation may, thereby accounting for the high position of ${}^{\phi}U_i = \gamma_{\phi E}$ relative to ${}^{h}U_i = \gamma_{hE}$ for air on the energy diagram in Fig. 8.

(ii) Open, free-surface states. This is the realm of surface physics and chemistry. The free surfaces at the rear edge of the crack adhesion zone are assumed to be in thermal equilibrium with the environment. The associated energy states may be obtained from $U_f = 2\gamma_B - 2\Delta U_{Ad}$ in Eq. (4) using the Gibbs adsorption equation[26]

$$\Delta U_{Ad} = kT \int_0^{p_E} \Gamma(p_E)\, dp_E/p_E \qquad (6)$$

where k is Boltzmann's constant, T the absolute temperature, Γ the excess concentration of the active species E at a B-E interface, and p_E the activity (partial pressure for gases) of this species. To evaluate Eq. (6) we must specify an appropriate isotherm relation. We defer explicit consideration of such a relation to a separate study.[24] It is well to recognize that the requirement for thermal equilibrium at the open interface may not always be met, in which case the free surface states (like their H and Φ interfacial counterparts on the right of Fig. 8) may be metastable. Such metastable states might arise if, for instance, the adsorption interaction at the surfaces were to be augmented by a competitive (if slow) corrosion process. In this context, aqueous solutions are indeed known to leach potassium ions from the mica surface[25,34] (perhaps accounting for our difficulty in obtaining healing in water).

The principal appeal of such an energy-level diagram lies in its clear representation of critical (stable or metastable) equilibrium fracture elements as well-defined end-point energy states. The construction may be used in a graphic way to predict the response of cracks with a "mixed" environmental history. As an illustration, consider virgin cracks at threshold loading in air, say, exposed subsequently to nitrogen gas or vacuum. Under these circumstances the threshold condition in the v-G function changes from $G = U_f(\text{air, RH } 55\%) = 608 \pm 56\ \text{mJ} \cdot \text{m}^{-2}$ to $G = U_f(\text{N}) \approx 1500 \pm 500\ \text{mJ} \cdot \text{m}^{-2}$, in which case the crack should spontaneously retract and heal [recall inverse relation between G and c in Eq. (3)]. We have observed this kind of healing behavior in our experiments. A more quantitative study of such healing phenomena requires careful attention to potential complications from transient states associated with the persistent presence of species from preceding environments in the adhesion zone.

As a second illustrative example, consider a specimen cleaved, mismatched, and healed in air, then split in liquid water. According to Fig. 8, the work of adhesion is then given by ${}^{\phi(\text{air})}\mathbf{W}_{W(L)} = U_f(\text{water}) - {}^{\phi}U_i(\text{air}) = (276 \pm 55) - (373 \pm 86) = -97 \pm 141\ \text{mJ} \cdot \text{m}^{-2}$. Notwithstanding the large scatter, this result suggests that the combination of misorientation and subsequent interaction might be sufficient to negate a large amount of the adhesion. It implies that mechanical histories which involve the opening and closing of cleavage fissures in air could even render ordinarily inert mica unstable to aqueous solutions (i.e., ${}^{\phi(\text{air})}\mathbf{W}_{W(L)} < 0$). As noted previously, we were unable to measure any adhesion from our experiments on mismatched mica.

The considerations of the two preceding paragraphs are specially relevant to the interpretation of mica-mica adhesion energies made by measuring pulloff loads between adhering contacts in the crossed-cylinder apparatus.[35] We would assert that there is a strong complementarity between the brittle crack and adhesive contact configurations, since both configurations are ostensibly governed by the same surface forces. For instance, a positive adhesion energy $\approx 5\ \text{mJ} \cdot \text{m}^{-2}$ is measured for mica in water in the crossed-cylinder experiment.[35] This value lies in the "noise" of the above result ${}^{\phi(\text{air})}\mathbf{W}_{W(L)} = -97 \pm 141\ \text{mJ} \cdot \text{m}^{-2}$ for mismatched interfaces from the

fracture data, but is significantly lower than ${}^{\circ}\mathbf{W}_{W(L)} = 276 \pm 55$ mJ · m^{-2} measured for virgin interfaces (Table I). In making such comparisons, it is important to realize that specimen preparation in the adhesion experiment conforms most closely to the mismatched fracture configuration: cleavage to full separation in air followed by recontact in arbitrary crystallographic orientation in subsequent test environment. We might go on to argue that, of the two complementary configurations, fracture is the only one capable of measuring surface energies of virgin solids, for there can be no guarantee that recontacted surfaces will ever completely restore the primary bonding ground state. Even experiments in which meticulous care is taken to orient the mica halves in perfect angular registry produce adhesion energies of 10–15 mJ · m^{-2} in water,[36] still far short of the 276 ± 55 mJ · m^{-2} for virgin cracks in Table I. This last result would appear to reinforce our earlier suggestion that aqueous solutions (in contrast to their atmospheric counterparts) may irreversibly alter the mica surfaces. Our considerations would also suggest that the pulloff force for adhering bodies must generally depend on whether the test environment is introduced before or after making contact.

The question may be raised as to the applicability of the energy-level concept to other solids. Similar deleterious effects of moisture on fracture properties have been reported in crack growth studies by Wiederhorn in glass[37] and sapphire.[38] Some efforts have also been made to quantify the energetics of healed interfaces in the first of these two materials.[39–41] (We have already mentioned the qualitative electron microscopy observations of healing in sapphire by Hockey.) Theoretical consideration of the "lattice structure" of crack interfaces in such solids[4] presents much the same picture as in Fig. 6, that of confined interfaces whose adhesion is ultimately determinable by oscillatory surface force functions. It is this physical picture that underlies our interpretation of velocity thresholds as manifestations of end-point equilibrium states, notwithstanding that the metastable states in glass and sapphire are likely to be dominated by *chemi*sorptive processes. Ultimately, we may envisage extension of the concept to more complex systems, e.g., systems with unlike materials A and B on either side of the interface [in which case we should have to replace Eq. (4) with a relation of the form ${}^{\circ}\mathbf{W}_{AEB} = \gamma_{AE} + \gamma_{BE} - \gamma_{AB}$]. Such would apply, for example, to the fracture of a polycrystalline material along an interphase boundary, or to the adhesive contact between a compliant sphere and rigid substrate.

One more issue may be raised here. Our analysis pertains to noncondensable fluids. If a capillary were to form at the interface, the analysis would require modification. Capillary condensation is a considerably more complex interfacial problem, which is currently receiving our attention.[42]

C. Kinetics

Finally, mention may be made of the kinetic processes responsible for the *v*-*G* curve. The implications of these kinetics extend beyond brittle fracture. We have already noted the fundamental complementarity between crack and adhesion problems: it follows that we should be able to use the results in Figs. 2–4 to predict not only the existence, but also the extent, of time-dependent behavior in adhesive contacts. It is perhaps surprising that kinetics have received so little attention in the fracture literature on mica. The Russian school noted the existence of a kinetic curve, and associated it with the leakage rate of the electrostatic charge on the crack walls (e.g., by surface charge transfer, electron emission, gas discharge).[20] However, consideration of the atomically discrete structure of the near-tip crack profile leads us to argue that transport of interactive species to the adhesion zone is a more plausible rate-controlling process.[4] We recall our earlier discussion of the confined crack interface in Fig. 6, in which we anticipated a significant pseudo-lattice diffusional resistance to the intrusion of environmental species. A simplistic calculation based on activation over corresponding lattice energy barriers[5] leads to a hyperbolic sine *v*-*G* function with linear argument in the *net* crack-extension force $G - \mathbf{W}$, consistent with the Griffith energy-balance thesis: increasing G incrementally above $\mathbf{W}$ opens the crack beyond its equilibrium configuration, thereby enhancing the forward diffusion of molecules; decreasing G below $\mathbf{W}$ likewise enhances the backward diffusion. This function applies to the steep portions of the curves in the semi-logarithmic *v*-*G* plots in Figs. 2–4, providing us with some theoretical justification for the extrapolation and interpolation procedure adopted in Sec. III for evaluating thresholds. At greater deviations from threshold alternative diffusional processes, less dependent on G, can become rate-limiting. The plateaus in the curves for the water vapor environments are attributable to free molecular flow along the more open crack interface behind the adhesion zone.[43]

A detailed analysis of such processes and their dependence on chemical composition (relative humidity), temperature, etc. on mica and other brittle materials will be presented elsewhere.[24]

V. CONCLUSION

Brittle fracture presents itself as a means for studying the energetics of surface-surface interactions. As such, it could prove a useful complement to the crossed-cylinder adhesion apparatus. Indeed, with regard to closed-interface states, the fracture experiment can provide information on the primary bonding (O) state that is usually inaccessible in the crossed-cylinder experiment: the latter experiment is inevitably re-

stricted to mismatched (Φ) or, with extreme care in alignment of opposing mica sheets, healed (H) states.[36]

ACKNOWLEDGMENTS

The authors are grateful to D. T. Smith, R. M. Thomson, and D. H. Roach for many stimulating discussions, to F. Scire for designing the apparatus shown schematically in Fig. 1, and to J. Fuller for preparing the mica specimens. Funding was provided by the United States Office of Naval Research, Ceramics and Metallurgy Program.

REFERENCES

[1]B. R. Lawn, Appl. Phys. Lett. **47**, 809 (1985).
[2]D. R. Clarke, B. R. Lawn, and D. H. Roach, in *Fracture Mechanics of Ceramics*, edited by R. C. Bradt, A. G. Evans, D. P. H. Hasselman, and F. F. Lange (Plenum, New York, 1986), Vol. 8, p. 341.
[3]D. H. Roach, D. M. Heuckeroth, and B. R. Lawn, J. Colloid and Interface Sci. **114**, 292 (1986).
[4]B. R. Lawn, D. H. Roach, and R. M. Thomson, J. Mater. Sci. **22**, 4036 (1987).
[5]B. R. Lawn and S. Lathabai, Mater. Forum **11**, 313 (1988).
[6]D. Maugis, J. Mater. Sci. **20**, 3041 (1985).
[7]B. R. Lawn and T. R. Wilshaw, *Fracture of Brittle Solids* (Cambridge University Press, London, 1975).
[8]J. N. Israelachvili, *Intermolecular and Surface Forces* (Academic Press, London, 1985).
[9]R. G. Horn and J. N. Israelachvili, J. Chem. Phys. **75**, 1400 (1981).
[10]D. Y. C. Chan and R. G. Horn, J. Chem. Phys. **83**, 5311 (1985).
[11]J. W. Obreimoff, Proc. Roy. Soc. Lond. **A127**, 290 (1930).
[12]B. V. Derjaguin, N. A. Krotova, and V. V. Karasev, Sov. Phys.–Dokl. **1**, 466 (1956).
[13]B. V. Derjaguin and M. S. Metsik, Sov. Phys.–Solid State **1**, 1393 (1960).
[14]A. I. Bailey, J. Appl. Phys. **32**, 1407 (1961).
[15]P. J. Bryant, in *Transactions of Ninth National Vacuum Symposium* (Macmillan, New York, 1962), p. 311.
[16]P. J. Bryant, L. H. Taylor, and P. L. Gutshall, in *Transactions of Tenth National Vacuum Symposium* (Macmillan, New York, 1963), p. 21.
[17]A. I. Bailey and S. M. Kay, Proc. Roy. Soc. Lond. **A301**, 47 (1967).
[18]A. I. Bailey and A. G. Price, J. Chem. Phys. **53**, 3421 (1970).
[19]R. B. Leonesio, J. Am. Ceram. Soc. **55**, 437 (1972).
[20]M. S. Metsik, J. Adhesion **3**, 307 (1972).
[21]A. I. Bailey and H. Daniels, J. Phys. Chem. **77**, 501 (1973).
[22]G. Trott, P. L. Gutshall, and J. M. Phillips, in *Proceedings of Seventh International Vacuum Congress and Third International Conference on Solid Surfaces*, Vienna, 1051 (1977).
[23]W. L. Bragg and G. F. Claringbull, *Crystal Structures of Minerals* (Bell, London, 1965), Vol. IV.
[24]K-T. Wan, S. Lathabai, and B. R. Lawn (to be published).
[25]D. H. Roach, S. Lathabai, and B. R. Lawn, J. Am. Ceram. Soc. **71**, 97 (1988).
[26]A. W. Adamson, *Physical Chemistry of Surfaces* (John Wiley, New York, 1982).
[27]E. Orowan, Nature **154**, 341 (1944).
[28]R. M. Pashley and J. N. Israelachvili, J. Colloid Interface Sci. **101**, 511 (1984).
[29]B. J. Hockey, in *Fracture Mechanics of Ceramics*, edited by R. C. Bradt, A. G. Evans, D. P. H. Hasselman, and F. F. Lange (Plenum, New York, 1983), Vol. 5, p. 637.
[30]G. L. Gaines and D. Tabor, Nature **178**, 1304 (1956).
[31]D. R. Clarke, J. Am. Ceram. Soc. **70**, 15 (1987).
[32]R. M. Thomson, Acta Metall. (to be published).
[33]D. Wolf and R. Benedek, in *Grain Boundary Phenomena in Electronic Ceramics: Advances in Ceramics, Vol. 1*, edited by L. M. Levinson (The American Ceramic Society, Columbus, OH, 1981), p. 107.
[34]R. M. Pashley, J. Colloid Interface Sci. **83**, 531 (1981).
[35]R. G. Horn, J. N. Israelachvili, and F. Pribac, J. Colloid Interface Sci. **115**, 480 (1987).
[36]P. M. McGuiggan and J. N. Israelachvili, Chem. Phys. Lett. **149**, 469 (1988).
[37]S. M. Wiederhorn, J. Am. Ceram. Soc. **50**, 407 (1967).
[38]S. M. Wiederhorn, in *Fracture of Ceramics*, edited by J. B. Wachtman, National Bureau of Standards Special Technical Publication 303, 217 (1969).
[39]G. L. Cheeseman and B. R. Lawn, Phys. Status Solidi (A) **3**, 951 (1970).
[40]B. Stavrinidis and D. G. Holloway, Phys. Chem. Glasses **24**, 19 (1983).
[41]E. R. Fuller and T. M. Michalske, J. Am. Ceram. Soc. **68**, 586 (1965).
[42]K-T. Wan and B. R. Lawn (to be published).
[43]B. R. Lawn, Mater. Sci. Eng. **13**, 277 (1974).